Chinese Chemical Letters 34 (2023) 107835

Contents lists available at ScienceDirect

Chinese Chemical Letters

journal homepage: www.elsevier.com/locate/cclet

Evolving a novel red-emitting two-photon dye with optically tunable amino group for monitoring the degree of hypoxia during liver fibrosis

Xingxing Zhang, Feiyu Yang, Tianbing Ren*, Yingxin Zheng, Xiao-Bing Zhang, Lin Yuan*

State Key Laboratory of Chemo/Biosensing and Chemometrics, College of Chemistry and Chemical Engineering, Hunan University, Changsha 410082, China

ARTICLE INFO

Article history:
Received 26 May 2022
Revised 14 September 2022
Accepted 14 September 2022
Available online 17 September 2022

Keywords:
Fluorescent probes
Two-photon imaging
Fluorophores
Nitroreductase
Hypoxia

ABSTRACT

Two-photon imaging has attracted increasing attention owing to its deep tissue imaging capabilities. Therefore, many fluorophores have been developed to satisfy its requirements. However, long-wavelength emission fluorophores with an optically tunable group are rarely developed. In this study, two long-wavelength emission fluorophores with an optically tunable amino group were successfully developed by introducing strong electron acceptor and large conjugated group to the TPQL dye. TPCO2 displayed a bright red emission ($\lambda_{em} = 638$ nm, $\Phi = 0.15$) together with high two-photon action cross section and good water solubility, which enabled higher signal-to-background ratios and deep tissue imaging. The proof-of-concept probe (TPCO–NO_2) was successfully applied to the high signal-to-background ratio imaging of nitroreductase in liver fibrosis, further realizing diagnosis of the degree of hypoxia during liver fibrosis.

The development of imaging technology, such as fluorescent imaging, which can perform non-invasive visual diagnosis of diseases *in vivo*, is playing an increasingly important role in biomedicine [1–3]. Traditional fluorophores including coumarin, BODIPY, fluorescein, and rhodamine, have been widely used for fluorescence imaging and sensing. However, most of them are usually one-photon (OP) excited by a UV–visible laser, with a wavelength in the range of 350–650 nm [4–10]. Compared with OP imaging, two-photon (TP) imaging can provide deeper tissue imaging with high spatial and temporal resolution owing to its near-infrared (NIR, 700–1000 nm) excitation [11–16]. Therefore, chemists have made significant efforts to develop new TP fluorophores with desirable photophysical performance, such as longer absorption/emission wavelengths and high fluorescence quantum yields, for imaging and sensing in living systems.

Although the excitation wavelength of TP imaging is in the NIR region, the emission wavelength of currently widely used TP fluorophores (*e.g.*, Acedan and naphthalimide derivantives) is concentrated in the range of 450–550 nm [17–20]. Within this region, intrinsic biomolecules in the tissues such as NADH, riboflavins, retinol, and folic acid, would cause serious autofluorescence [21–24]. In recent years, several studies have been devoted to developing novel long-wavelength emitting TP fluorophores [25,26]. Among them, π-extended Acedan analogues and DCM dyes are popular for TP probe design owing to their structural modifiability (Scheme 1A) [27–29]. However, these fluorophores still suffer from some weaknesses, such as a lack of optically tunable groups [29], sensitivity to pH, and poor solubility [30,31]. Therefore, the development of excellent long-wavelength TP fluorophores with optically tunable groups for *in vivo* molecular imaging remains a challenge.

Herein, by introducing strong electron acceptor and large conjugated group to the TPQL dye, we designed and synthesized two long-emission TP fluorophores (TPCN1 and TPCO2) with an optically tunable amino group (Scheme 1B). Importantly, TPCO2 displayed a bright red emission ($\lambda_{em} = 638$ nm, $\Phi = 0.15$ in EtOH) together with a high two-photon action cross section (61 GM at 810 nm) and good water solubility, which enabled high signal-to-background ratios and deep tissue imaging. To demonstrate this versatility, we designed and synthesized two activatable TP probes: TPCO–N_3 and TPCO–NO_2. The optical properties study demonstrated that TPCO–N_3 and TPCO–NO_2 can rapidly, highly selectively, and sensitively response to H_2S and nitroreductase (NTR), respectively. Using probe TPCO–NO_2, we not only successfully distinguished the expression of NTR in cells under different hypoxic conditions, but also sensitively imaged the NTR expression levels in liver fibrosis, further realizing diagnosis of the degree of hypoxia during liver fibrosis progression.

In a previous work, we have developed well-behaved two-photon dyes TPQLs with an optically tunable amino group [13].

* Corresponding authors.
E-mail addresses: rentianbing@hnu.edu.cn (T. Ren), lyuan@hnu.edu.cn (L. Yuan).

https://doi.org/10.1016/j.cclet.2022.107835
1001-8417/

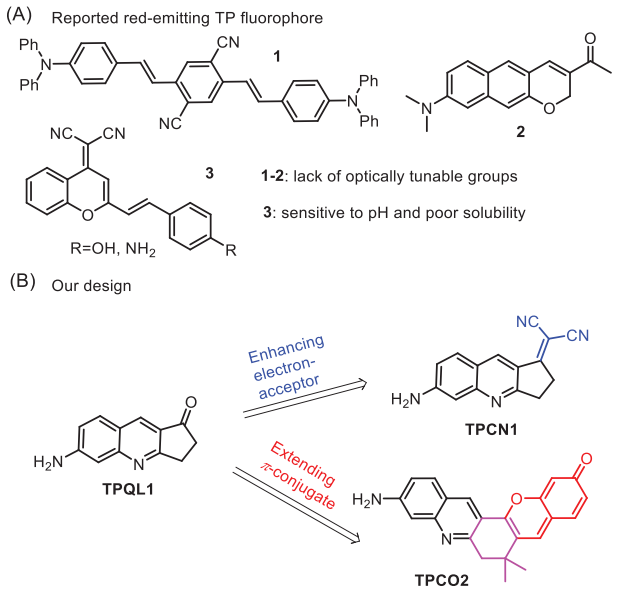

Scheme 1. (A) The reported red-emitting TP fluorophores. (B) Our design of TP fluorophores with longer emission wavelength.

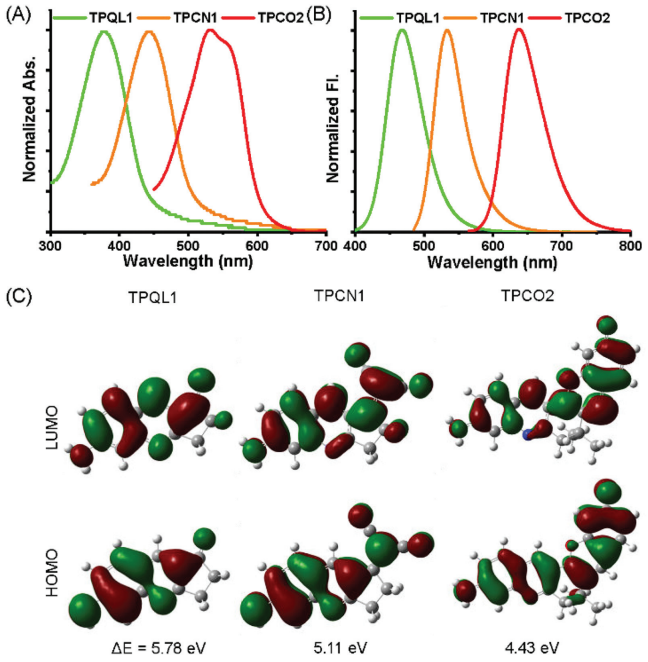

Fig. 1. Normalized absorption (A) and fluorescence emission (B) spectra of TPQL1, TPCN1 and TPCO2 in ethanol. (C) Optimized frontier molecular orbitals and orbital energies gap of TPQL1, TPCN1 and TPCO2 in the excited state.

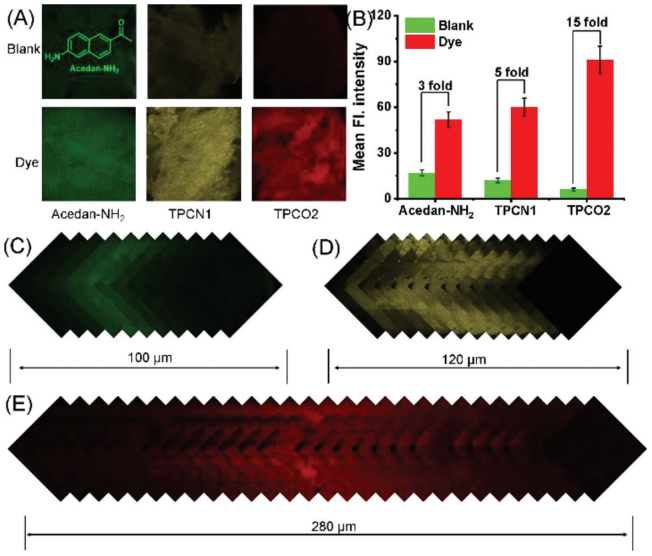

Fig. 2. Confocal TP fluorescence images of liver tissues. (A) Liver tissues cultured with TPCO2, Acedan-NH_2 and TPCN1. TPCO2: λ_{ex} = 810 nm, λ_{em} = 663–738 nm; Acedan-NH_2: λ_{ex} = 750 nm, λ_{em} = 425–475 nm; TPCN1: λ_{ex} = 810 nm, λ_{em} = 500–550 nm; Scale bar = 50 μm; Laser power is 3 mW. (B) mean fluorescence intensity and signal-to-background ratio of A. (C-E) Tissue depth of Acedan-NH_2, TPCN1 and TPCO2.

However, their emission wavelengths were still short. Currently, attempts to obtain long-wavelength fluorophores have focused mainly on molecular engineering strategy by expanding the π-conjugate structure and introducing strong electron-donating (D) and electron-accepting (A) groups [32–34]. Thus, we intended to introduce malononitrile (a strong electron acceptor) and a phenol derivative (a large conjugated group) into the TPQL to afford novel long-wavelength emitting TP dyes (Scheme 1B). As design in Scheme S1 (Supporting information), TPCN1 and TPCO1 were to be synthesized by a simple one-step method. However, owing to the high rigidity of the five-membered ring (Figs. S1a and b in Supporting information), the enlarged conjugated dye TPCO1 was not successfully synthesized. Finally, we synthesized dye TPCO2 with a twisted six-membered ring (Figs. S1c and d in Supporting information). Both TPCN1 and TPCO2 were characterized by NMR analyses. Subsequently, their photophysical properties were studied in different solvents. As shown in Fig. 1, Figs. S2 and S3 (Supporting information), compared to TPQL1 ($\lambda_{abs}/\lambda_{em}$ = 395/475 nm), by introducing a strong electron acceptor, the maximum absorption (λ_{abs}) and emission (λ_{em}) wavelengths of TPCN1 exhibited only a red-shift of approximately 50 nm, reaching 442/533 nm. However, when the π-conjugate structure was extended, the emission wavelength of TPCO2 showed a red-shift more than 150 nm, up to 638 nm. These results indicated that expanding the π-conjugation is more suitable for substantially red-shifting the wavelength of dye. This conclusion was verified by density functional theory (DFT) calculations (Fig. 1C). Furthermore, it should be noted that, with the solvent changing from dichloromethane to water, the emission wavelength of the new dyes shifted only approximately 12 nm (TPCN1) and 18 nm (TPCO2) (Fig. S4 in Supporting information), which indicated their environmental insensitivity. In addition, the high quantum yield, good water solubility, and pH insensitivity showed great potential for biological imaging (Table S1, Figs. S5 and S6 in Supporting information).

The two-photon absorption cross section was a key feature of TP fluorophores. Therefore, the fluorophores were investigated in PBS buffer. As shown in Fig. S7 (Supporting information), TPCN1 and TPCO2 exhibited the broadest two-photon action cross sections of 82 and 61 GM at 810 nm, respectively. To further evaluate the TP efficiency of the new dyes, TP fluorescence imaging was compared using live tissues. The tissues were incubated with TPCO2 (10 μmol/L), TPCN1 (10 μmol/L), or Acedan-NH_2 (10 μmol/L) for 30 min. Emission signals were collected and imaged using TP microscopy. The intensity of the background fluorescence of the red light was much lower than that of the green and yellow light under the same laser power. Therefore, the imaging signal-to-background ratio of TPCO2 (15 folds) was much higher than those of Acedan-NH_2 (3 folds) and TPCN1 (5 folds). Z-scan imaging of live tissues also revealed that TPCO2 displayed deeper tissue penetration (280 μm) than Acedan-NH_2 (160 μm) or TPCN1 (120 μm) (Fig. 2).

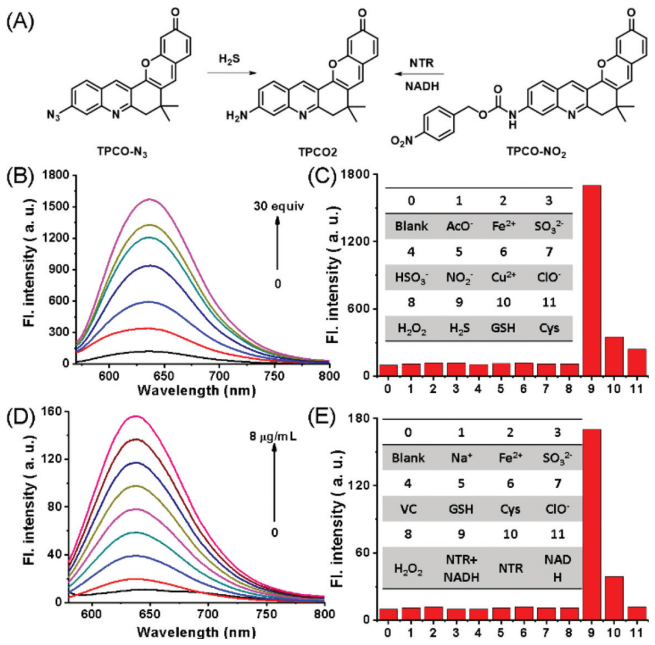

Fig. 3. (A) Structure of TPCO–N_3 and TPCO–NO_2 and its response mechanism to H_2S and NTR. (B) Fluorescence spectra of TPCO–N_3 in the presence of H_2S for 10 min. (C) Fluorescence responses of TPCO–N_3 to various species in PBS (pH 7.4) buffer solution at 37 °C for 10 min. (D) Fluorescence spectra of TPCO–NO_2 in the presence of NTR with 500 μmol/L NADH in PBS (pH 7.4) buffer solution at 37 °C for 60 min. (E) Fluorescence responses of TPCO–NO_2 to various species in PBS (pH 7.4) buffer solution at 37 °C for 60 min. $\lambda_{ex} = 525$ nm, $\lambda_{em} = 570–800$ nm.

Considering its long-emission wavelength and high QY, we chose TPCO2 for further study. First, we performed MTT assay. When the concentration of TPCO2 reached 50 μmol/L, the cells still showed a high viability (Fig. S8 in Supporting information). Next, we studied the photostability of TPCO2, and observed that TPCO2 still maintained a high brightness after 1 h of irradiation. In contrast, the brightness of Cy5 dropped to 80% of its initial value under the same conditions (Fig. S9 in Supporting information). Next, we studied the stability of TPCO2 in cells. Similar to the *in vitro* results, TPCO2 showed superior photostability in cells compared to Cy5. The fluorescence of Cy5 was nearly completely bleached after 10 min of illumination, however, TPCO2 remained at 50% of its original value (Fig. S10 in Supporting information). These results indicate that TPCO2 has better photostability than Cy5 and can be applied to long-term tracking imaging research.

To demonstrate that TPCO2 can be used in the design of activatable probes, two different types of probes were prepared by incorporating a 4-nitrobenzyl carbonochloridate group and azido group into TPCO2 to detect nitroreductase (NTR) and H_2S, respectively (Scheme S2 in Supporting information). Next, we investigated its responsiveness. The fluorescence of TPCO–N_3 was negligible. When H_2S was added at room temperature, it was reduced to TPCO2 (Fig. S11 in Supporting information), resulting in strong fluorescence (Figs. 3A and B). Selectivity experiments demonstrated the specificity of TPCO–N_3's response to H_2S (Fig. 3C and Fig. S12 in Supporting information). As shown in Fig. 3D, TPCO–NO_2 exhibits almost no fluorescence. When NTR and NADH were added, the fluorescence at 635 nm increased by 16.5 times. The selectivity of TPCO–NO_2 for the NTR was also evaluated. As shown in Fig. 3E, only when NTR and coenzyme NADH coexist, the fluorescence at 635 nm significantly increases, indicating TPCO–NO_2 has a higher selectivity for NTR. The above experiments showed that TPCO2 could be regarded as a platform for the design of activatable probes.

To verify its sensing ability, the reaction kinetics of TPCO–NO_2 with NTR were monitored. When NTR was added, fluorescence at 635 nm increased and reached saturation at approximately 60 min (Fig. S13 in Supporting information). Meanwhile, the higher the NTR concentration, the more obvious the fluorescence enhancement. When the NTR concentration reached 10 μg/mL, the fluorescence at 635 nm reached saturation (Fig. 3D). When the concentration of NTR was in the range of 0–8 μg/mL, the probe showed a good linear relationship and low detection limit (0.019 μg/mL), revealing a highly sensitive response to NTR. The above results demonstrated that TPCO–NO_2 had a good specific response to NTR, and was appropriate for monitoring NTR levels *in vitro*.

Hypoxia in human body leads to the overexpression of several intracellular reductases, including NTR [35]. Since TPCO–NO_2 can sensitively and selectively respond to NTR *in vitro*, it was used to differentiate NTR expression levels in different oxygen environments. MTT experiments showed that the probe had good biosafety and biocompatibility with HeLa cells (Fig. S8), and could be used for the imaging analysis of NTR in cells. HeLa cells were cultured in the presence of different concentrations of oxygen (21%, 10% and 1%). Then the cells were incubated with TPCO–NO_2 for 1 h, followed by fluorescence imaging (Fig. 4A). The fluorescence of the cells was weak under normoxia, indicating that the NTR was less expressed in the normal environment. As the oxygen concentration decreased, the fluorescence intensity increased, indicating that the expression of NTR increased with intensified anaerobic conditions of the cells (Figs. 4A and B). This demonstrated that TPCO–NO_2 could be applied to image the expression level of NTR under different oxygen environments. Therefore, the degree of hypoxia in organisms can be identified by analysing the expression levels of NTR.

Liver fibrosis develops in any etiology of chronic liver injury [36]. Currently, there is no effective treatment for liver fibrosis, which severely affects the life of patients. Recent studies have shown that hypoxia is an important factor in liver fibrosis [37]. Therefore, exploring the relationship between liver fibrosis and hypoxia can provide a theoretical basis for the analysis and treatment of this disease. Given the excellent sensitivity and selectivity of TPCO–NO_2, we used it to monitor the degree of hypoxia during liver fibrosis by detecting NTR. The liver fibrosis model was established by intraperitoneal injection of CCl_4 as previously described (Animal experiments were approved by the Animal Ethics Committee of College of Biology (Hunan University)). To monitor the degree of hypoxia during liver fibrosis, we set up two experimental groups, treated with CCl_4 for 2 and 4 weeks, respectively. All liver tissues were stained with TPCO–NO_2 (10 μmol/L) for two-photon microscopy imaging. Liver tissues from normal mice exhibited negligible fluorescence, reflecting the relatively low NTR expression in healthy mice (Fig. 4C). Meanwhile, the fluorescence intensity of the liver tissue in mice with liver fibrosis was significantly stronger (Fig. 4C). With the aggravation of liver fibrosis, fluorescence intensity significantly increased, indicating that hypoxia worsened as fibrosis progressed. Moreover, the penetration depth of TPCO–NO_2 reached 160 μm in a 4-week CCl_4-induced mice liver tissue (Fig. 4D). When the NTR inhibitor dicoumarol was added to liver fibrosis tissues, the tissues exhibited significantly weak fluorescence, indicating that TPCO–NO_2 can monitor the NTR activity and assess the degree of hypoxia (Figs. 4C and E). Considering the essential role of HIF-1α (hypoxia-inducible factor) in the progression of liver fibrosis [38–42], we further monitored the levels of HIF-1α in liver fibrosis tissues *via* ELISA. As shown in Fig. 4F, with the progression of liver fibrosis, HIF-1α level significantly increased. This data is consistent well with the fluorescence result, indicating that TPCO–NO_2 has the potential to be used for monitoring the liver fibrosis by hypoxia imaging.

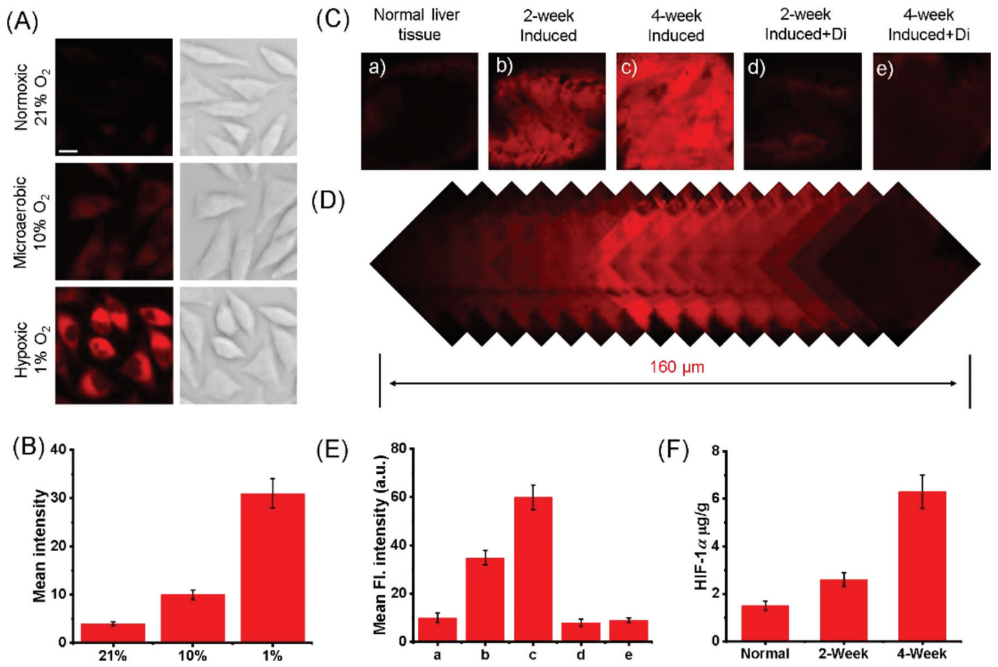

Fig. 4. (A) Fluorescence imaging of HeLa cells with different pretreatments before incubation with TPCO–NO_2 (10 μmol/L) by two-photon confocal imaging. Scale bar: 10 μm. (B) Relative fluorescence intensity in HeLa cells from A. (C) Two-photon microscopy imaging of TPCO–NO_2 (10 μmol/L) in liver fibrosis mice liver tissues. (D) Depth fluorescence images of TPCO–NO_2 in 4-week CCl_4 induced mice liver tissue. $\lambda_{ex} = 810$ nm, $\lambda_{em} = 663$–738 nm. (E) Quantification of the relative mean fluorescence levels of cells from the images of A. (F) Quantification of the concentrations of HIF-1α in the normal liver and fibrosis liver tissues by ELISA Kit.

In summary, we developed a novel red-emitting TP dye with an optically tunable amino group. TPCO2 displayed a bright red emission ($\lambda_{em} = 638$ nm, $\Phi = 0.15$) together with a high two-photon action cross section and good water solubility, which enabled high signal-to-background ratios and deep tissue imaging. Based on the favourable photophysical properties of TPCO2, we designed two different types of probes. The probe TPCO–NO_2 showed good selectivity, high sensitivity, and selectivity to NTR, and could realize the imaging of NTR expression in cells under different hypoxic conditions. More importantly, TPCO–NO_2 was successfully applied to high signal-to-background ratio imaging of NTR in liver fibrosis, further realizing the diagnosis of the degree of hypoxia during liver fibrosis. Therefore, TPCO2 can be used as a platform for designing activated TP probes.

Declaration of competing interest

The authors declare that they have no known competing financial interests or personal relationships that could have appeared to influence the work reported in this paper.

Acknowledgments

This work is supported by the National Natural Science Foundation of China (Nos. 22074036, 22004033, 21877029) and Special Funds for the Construction of Innovative Provinces in Hunan Province (No. 2019RS1031).

Supplementary materials

Supplementary material associated with this article can be found, in the online version, at doi:10.1016/j.cclet.2022.107835.

References

[1] T.B. Ren, W. Xu, W. Zhang, et al., J. Am. Chem. Soc. 140 (2018) 7716–7722.
[2] X. Fan, T. Ren, W. Yang, X. Zhang, L. Yuan, Chem. Commun. 57 (2021) 8644–8647.
[3] G. Jiang, T.B. Ren, E. D'Este, et al., Nat. Commun. 13 (2022) 2264.
[4] W. Xu, Z. Zeng, J.H. Jiang, Y.T. Chang, L. Yuan, Angew. Chem. Int. Ed. 55 (2016) 13658–13699.
[5] X. Chen, F. Wang, J.Y. Hyun, et al., Chem. Soc. Rev. 45 (2016) 2976–3016.
[6] D. Cao, Z. Liu, P. Verwilst, et al., Chem. Rev. 119 (2019) 10403–10519.
[7] J. Bai, J. Zhou, X. Ji, W. Zhao, et al., Chin. Chem. Lett. 33 (2022) 4175–4178.
[8] G. Hu, H. Jia, L. Zhao, D. Cho, J. Fang, Chin. Chem. Lett. 30 (2019) 1704–1716.
[9] X. Zhang, C. Wang, L. Jin, Z. Han, Y. Xiao, ACS Appl. Mater. Interfaces 6 (2014) 12372–12379.
[10] S. Pascal, S. David, C. Andraud, O. Maury, Chem. Soc. Rev. 50 (2021) 6613–6658.
[11] L. Wu, J. Liu, P. Li, B. Tang, T.D. James, Chem. Soc. Rev. 50 (2021) 702–734.
[12] L. Yuan, W. Lin, H. Chen, S. Zhu, L. He, Angew. Chem. Int. Ed. 52 (2013) 10018–10022.
[13] X. Zhang, T. Ren, Q. Zhang, et al., Cell Rep. Phys. Sci. 2 (2021) 100471.
[14] T.B. Ren, W. Xu, Q.L. Zhang, et al., Angew. Chem. Int. Ed. 57 (2018) 7473–7477.
[15] Y. Zheng, X.X. Zhang, L. Shi, et al., Chem. Asian J. 17 (2022) e202101197.
[16] X. Zhang, T. Ren, L. Yuan, et al., Chin. Chem. Lett. 32 (2021) 3890–3894.
[17] H.M. Kim, C. Jung, B.R. Kim, et al., Angew. Chem. Int. Ed. 46 (2007) 3460–3463.
[18] C. Zhang, P. Wang, X. Yin, et al., Anal. Chem. 91 (2019) 6371–6377.
[19] J. Ning, Z. Tian, J. Wang, et al., Angew. Chem. Int. Ed. 61 (2022) e202113191.
[20] H. Fang, R. Shi, D. Chen, et al., Chem. Commun. 57 (2021) 11260–11263.
[21] R. Zipfel Warren, M. Williams Rebecca, R. Christie, et al., Proc. Natl. Acad. Sci. U. S. A. 100 (2003) 7075–7080.
[22] S. Huang, A.A. Heikal, W.W. Webb, Biophys. J. 82 (2002) 2811–2825.
[23] A.J. Radosevich, M.B. Bouchard, S.A. Burgess, B.R. Chen, E.M.C. Hillman, Opt. Lett. 33 (2008) 2164–2166.
[24] C.H. Heo, K.H. Kim, H.J. Kim, et al., Chem. Commun. 49 (2013) 1303–1305.
[25] G. Niu, X. Zheng, Z. Zhao, et al., J. Am. Chem. Soc. 141 (2019) 15111–15120.
[26] X. Zhang, Kevin D. Belfield, Y. Xiao, J. Qi, J. Qu, et al., J. Org. Chem. 78 (2013) 9153–9160.
[27] D. Kim, H. Moon, S.H. Baik, et al., J. Am. Chem. Soc. 137 (2015) 6781–6789.
[28] M. Li, X. Wu, Y. Wang, et al., Chem. Commun. 50 (2014) 1751–1753.
[29] S. Singha, Y.W. Jun, S. Sarkar, K.H. Ahn, Acc. Chem. Res. 52 (2019) 2571–2581.
[30] K. Gu, Y. Xu, H. Li, et al., J. Am. Chem. Soc. 138 (2016) 5334–5340.
[31] T. Liu, M. Zhang, L. Feng, et al., Sens. Actuators B: Chem. 337 (2021) 129764.
[32] L. He, H. Xiong, B. Wang, et al., Anal. Chem. 92 (2020) 11029–11034.
[33] A. Gandioso, S. Contreras, I. Melnyk, et al., J. Org. Chem. 82 (2017) 5398–5408.
[34] S.S. Matikonda, J. Ivanic, M. Gomez, G. Hammersley, M.J. Schnermann, Chem. Sci. 11 (2020) 7302–7307.
[35] J. Brown, W. Wilson, Nat. Rev. Cancer 4 (2004) 437–447.
[36] E. Seki, D.A. Brenner, J. Hepato-Bil-Pan Sci. 22 (2015) 512–518.
[37] M. Fernandez, D. Semela, J. Hepatol. 50 (2009) 604–620.
[38] T. Kietzmann, E.Y. Dimova, D. Flügel, J.G. Scharf, Z. Gastroenterol. 44 (2006) 67–76.
[39] R. Kumari, D. Sunil, R.S. Ningthoujam, Bioorg. Chem. 88 (2019) 102979.
[40] D.J. Manalo, A. Rowan, T. Lavoie, et al., Blood 105 (2005) 659–669.
[41] E. Novo, S. Cannito, E. Zamara, et al., Am. J. Pathol. 170 (2007) 1942–1953.
[42] J. Cai, M. Hu, Z. Chen, Z. Ling, J. Transl. Med. 19 (2021) 186.